arXiv:1208.3098v1 [cond-mat.mtrl-sci] 15 Aug 2012

Confinement induced metal-to-insulator transition in strained $LaNiO_3/LaAlO_3$ superlattices

Ariadna Blanca-Romero[1] and Rossitza Pentcheva[1,*]
[1]*Department of Earth and Environmental Sciences, Section Crystallography and Center of Nanoscience, University of Munich, Theresienstr. 41, 80333 Munich, Germany*
(Dated: August 16, 2012)

Using density functional theory calculations including a Hubbard U term we explore the effect of strain and confinement on the electronic ground state of superlattices containing the band insulator $LaAlO_3$ and the correlated metal $LaNiO_3$. Besides a suppression of holes at the apical oxygen, a central feature is the asymmetric response to strain in single unit cell superlattices: For tensile strain a band gap opens due to charge disproportionation at the Ni sites with two distinct magnetic moments of $1.45\mu_B$ and $0.71\mu_B$. Under compressive stain, charge disproportionation is nearly quenched and the band gap collapses due to overlap of $d_{3z^2-r^2}$ bands through a semimetallic state. This asymmetry in the electronic behavior is associated with the difference in octahedral distortions and rotations under tensile and compressive strain. The ligand hole density and the metallic state are quickly restored with increasing thickness of the $(LaAlO_3)_n/(LaNiO_3)_n$ superlattice from $n = 1$ to $n = 3$.

PACS numbers: 73.20.-r,68.65.Cd,71.30.+h,74.78.Fk

The ability to grow transition metal oxide heterostructures with atomic control of layer thickness opens an exciting realm to explore confinement effects and novel effectively two-dimensional electronic phases that are not accessible in the bulk compounds. To this end, Chaloupka and Khaliullin[1] recently proposed that a cuprate-like behavior may be stabilized in a La_2NiMO_6 superlattice (SL) where NiO_2 and MO_2 planes alternate along the c-axis of the ABO_3 perovskite lattice and M denotes a trivalent cation (M=Al, Ga, Ti). $LaNiO_3$ is a perovskite compound with rhombohedral symmetry ($R\bar{3}c$) that remains metallic at all temperatures due to degenerate e_g orbitals at the Ni^{3+}-sites ($t_{2g}^6 e_g^1, S = 1/2$). In contrast to bulk LNO, all other representatives of the rare earth nickelates undergo a metal-to-insulator transition (MIT)[2] at low temperatures, driven by charge ordering (CO) rather than the Jahn-Teller effect.[3,4] Chaloupka and Khaliullin[1] proposed that the orbital degeneracy in LNO/LMO superlattices can be lifted and a selective $d_{3z^2-r^2}$ or $d_{x^2-y^2}$ occupation at the Ni^{3+} sites achieved by applying strain induced by the substrate. Subsequent density functional theory (DFT) calculations in the local density approximation (LDA) found a two sheet Fermi surface (FS) with strongly hybridized $d_{3z^2-r^2}$ and $d_{x^2-y^2}$ orbitals.[5,6] A single-sheet FS could only be obtained by including correlation effects within the dynamical mean field approximation (DMFT) and/or by using Sc as counterion to Ni instead of Al.[7] Han *et al.*[8] showed that the choice of the counterion (Al, Ga, B, In) rather than strain can be used to control chemically the orbital polarization.

The DFT studies mentioned above have considered exclusively superlattices in a tetragonal setup. However, both $LaNiO_3$ (LNO) and $LaAlO_3$ (LAO) are rhombohedral in the bulk (space group $R\bar{3}c$). Here we explore the effect of confinement and strain on the octahedral distortions. DFT calculations with an on-site Coulomb repulsion term show that the lattice distortions have a significant influence on the bandwidth and thereby on the electronic ground state of the system. In particular, a charge disproportionated (CD) insulating state is obtained in LAO_1/LNO_1 SLs under tensile strain. In a tetragonal cell such a state is reported only at higher U values.[7] The tendency toward CD is vastly suppressed under compressive strain.

A metal-to-insulator transition as a function of LNO thickness has been observed experimentally for $LaNiO_3/LaAlO_3$[9,10] and $LaNiO_3/SrMnO_3$[11] superlattices as well as in thin LNO films grown on an STO(001) substrate.[12,13] The Ruddlesden-Popper compound $La_4Ni_3O_8$[14,15] is another example for an insulating state due to confinement. Here, we explore the effect of quantum confinement by varying the period of the $(LAO)_n/(LNO)_n$ superlattice from $n = 1$ to $n = 3$. The results show a quick convergence toward bulk metallic behavior within the LNO part of the superlattice with increasing thickness.

I. CALCULATIONAL DETAILS

To gain insight into the electronic behavior of $(LAO)_n/(LNO)_n$ ($n = 1, 3$) superlattices, we performed density functional theory calculations with the full potential linearized augmented plane wave method as implemented in the WIEN2k code.[16] An on-site Coulomb repulsion term is considered beyond the generalized gradient approximation[17] of the exchange correlation potential within the LDA/GGA+U approach[18] using $U = 4$ eV and $J = 0.7$ eV for Ni and $U = 7$ and $J = 0$ eV for La. The muffin tin (MT) radii are 1.80 bohrs (Ni and Al), 2.30 bohrs (La) and 1.60 bohrs (oxygen). Inside the muffin tins, wave functions are expanded in spherical harmonics up to $l_{\max}^{\mathrm{wf}} = 10$ and nonspherical contributions to the electron density and potential are considered up to $l_{\max}^{\mathrm{pot}} = 6$. The energy cutoff for the plane wave representation in the interstitial is $E_{\max}^{\mathrm{wf}} = 25$ Ry for the wave functions and $E_{\max}^{\mathrm{pot}} = 144$ Ry for the potential. 76 k-points were used for the integration in the irreducible part of the Brillouin zone (BZ). To model the effect of substrate- induced strain, the in-plane lattice parameter of the superlattice was set to that of LAO ($a = 3.78$Å), STO ($a = 3.905$Å) or $DyScO_3$ (DSO) ($a = 3.94$Å), respectively. For the out-of-plane parameter we have used values obtained from XRD measurements: 3.83 (STO) and 3.93 Å (LAO).[19] Relaxations of the c parameter for superlattices strained at a_{DSO} rendered a c value very similar to the one for the STO case. This implies a deviation from the volume conserving scenario for tensile strain, as also suggested from XRD measurements.[19] While previous DFT studies[5,8] have used a tetragonal setup, we explored the influence of strain on the octahedral rotations by optimizing the internal parameters in a monoclinic unit cell containing 20 atoms for LNO bulk and the 1/1 superlattice. In the present study parallel alignment of the Ni spins is considered. Calculations for antiferromagnetic configurations were unstable and higher in energy.

II. BULK LNO

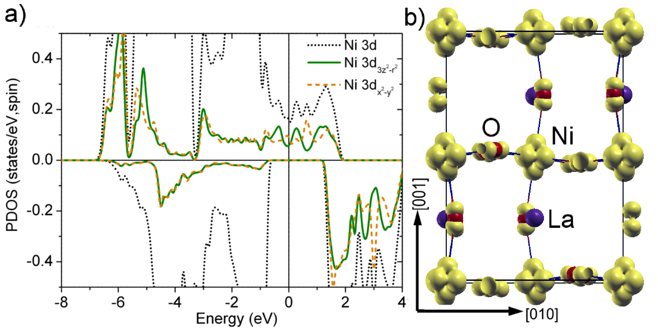

FIG. 1: (Color online) Bulk LaNiO$_3$. (a) Projected density of states of Ni 3d character (black dotted line) obtained within GGA+U ($U = 4$ eV and $J = 0.7$ eV). Positive (negative) values correspond to majority (minority) spin. Note that $d_{3z^2-r^2}$ (green line) and $d_{x^2-y^2}$ orbitals (orange dashed line) are degenerate in bulk LNO. (b) Electron density distribution of the unoccupied states integrated between E$_F$ and E$_F$+2.5 eV. La and O ions are denoted by purple and red spheres, respectively.

Prior to studying the LAO/LNO superlattices we investigate here the electronic properties of LNO bulk. In order to facilitate comparison to the LNO/LAO superlattices the calculations are performed in a monoclinic unit cell containing 20 atoms. Figure 1(a) shows the projected density of states at the Ni sites. In bulk LNO $d_{3z^2-r^2}$ and $d_{x^2-y^2}$ are degenerate and the broad e_g band extends from -7 eV to 2 eV in the majority spin channel, while the minority e_g states are not occupied except for some hybridization with the O 2p states between -4.5 and -3.5 eV. The formal Ni valence in LNO is considered to be Ni^{3+} (t_{2g}^6,e_g^1), but the occupation of the Ni e_g states is much higher (both the $d_{3z^2-r^2}$ and $d_{x^2-y^2}$ orbtails contain one electron each; see Table I). As displayed in the hole density distribution integrated between $E_{\rm F}$ and $E_{\rm F} + 2.5$ eV [Fig 1(b)], the higher number of electrons at the Ni sites is counterbalanced by holes on the ligands of p_σ character ($\sim 0.2e$ within the MT). This corresponds to a state closer to 3d^8L, where L denotes a hole on the oxygen site, as observed also for other rare-earth nickelates.[20] For this reason bulk LaNiO$_3$ was ruled out as a possible parent compound for high-Tc superconductivity.[21]

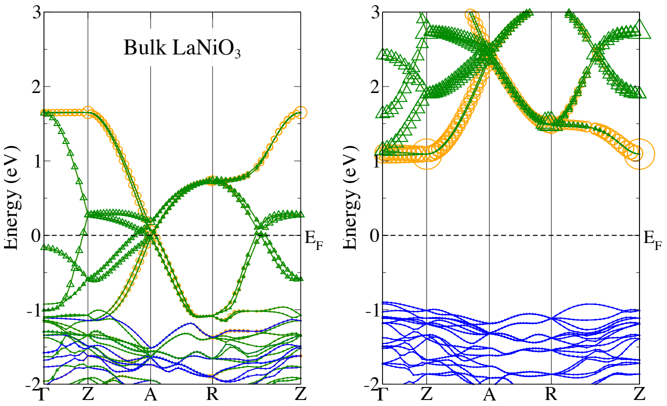

(a) Majority spin channel

(b) Minority spin channel

FIG. 2: (Color online) Band structure obtained within GGA+U of bulk LaNiO$_3$ along the high symmetry lines $\Gamma(0,0,0)-Z(0,0,\pi)-A(\pi,0,\pi)-R(\pi,\pi,\pi)-Z(0,0,\pi)$ using a $\sqrt{2}a\times\sqrt{2}a\times 2a$ unit cell with a being the lattice parameter of the pseudocubic cell. In (a) and (b) the $d_{3z^2-r^2}$ and $d_{x^2-y^2}$ character is emphasized by green triangles and light orange circles, respectively.

The band structure of bulk LNO in Fig. 2 is plotted along the high-symmetry lines in the BZ of the 20-atom cell. We concentrate on the antibonding e_g bands in the majority spin channel extending from -1 eV to 2 eV (in the minority spin channel these states are empty). At Γ both e_g bands are degenerate, $d_{3z^2-r^2}$ bands show a strong dispersion along $\Gamma-Z$, while $d_{x^2-y^2}$ bands are dispersive mainly along $Z-A-R-Z$. Both bands cross $E_{\rm F}$ at A and $d_{3z^2-r^2}$ also halfway along $R-Z$.

III. LAO/LNO SUPERLATTICES: ELECTRONIC PROPERTIES

A. (LaAlO$_3$)$_1$/(LaNiO$_3$)$_1$ superlattices

We now turn to the (LaAlO$_3$)$_1$/(LaNiO$_3$)$_1$ superlattices strained at the lateral lattice parameters of LAO, STO, and DSO. Their total density of states (DOS) are plotted in Fig. 3 together with the one for bulk LNO. For compressive strain (short-dashed cyan line) the system is (semi-)metallic with a dip of DOS at the Fermi level. Moreover, due to the stacking of insulating LAO and conducting LNO layers an enhanced resistivity is expected for (LaAlO$_3$)$_1$/(LaNiO$_3$)$_1$ at $a_{\rm LAO}$. In contrast, for tensile strain a gap in the total density of states (Fig. 3) of 0.3 eV occurs above the Fermi level (solid line, gaey area). Interestnigly, the total DOS of (LaAlO$_3$)$_1$/(LaNiO$_3$)$_1$ at $a_{\rm DSO}$ almost coincides with the one for $a_{\rm STO}$ around the Fermi level, implying a nonlinear dependence of the electronic properties on strain. Therefore, we concentrate in the following on the electronic properties of (LaAlO$_3$)$_1$/(LaNiO$_3$)$_1$ strained at $a_{\rm LAO}$ and $a_{\rm STO}$.

TABLE I: Orbital occupation (total and majority/minority spin) of Ni e_g states in (LAO)$_n$/(LNO)$_n$ strained at $a_{\rm STO}$ (tensile), $a_{\rm LAO}$ (compressive), and $a_{\rm DSO}$ (tensile) compared to Ni in bulk LNO. The lateral strain with respect to the bulk LNO lattice parameter a_0 is $\epsilon = (a - a_0)/a_0$. Additionally, the orbital polarization of the occupied e_g states $P = (n_{x^2-y^2} - n_{3z^2-r^2})/(n_{x^2-y^2} + n_{3z^2-r^2})$ and the magnetic moments are displayed. The last two columns give the number of holes Δp_σ (difference in occupation with respect to the fully occupied p_π orbitals) of the apical (a) and basal (b) oxygen within the MT sphere.

		$n_{3z^2-r^2}$	$n_{x^2-y^2}$	P[%]	M [$\mu_{\rm B}$]	Δp_σ^a	Δp_σ^b
1/1@$a_{\rm LAO}$	Ni1	1.06 (0.86/0.19)	0.98 (0.76/0.22)	-3.8	1.22	-0.10	-0.19
ϵ =-1.1%	Ni2	1.02 (0.77/0.24)	0.98 (0.72/0.26)	-1.6	0.98	-0.13	-0.19
1/1@$a_{\rm STO}$	Ni1	1.05 (0.87/0.18)	1.02 (0.86/0.15)	-1.7	1.45	-0.09	-0.22
ϵ =1.7%	Ni2	0.97 (0.63/0.33)	1.01 (0.71/0.30)	2.2	0.71	-0.15	-0.22
1/1@$a_{\rm DSO}$	Ni1	1.05 (0.87/0.18)	1.02 (0.87/0.14)	-1.7	1.47	-0.09	-0.22
ϵ =2.7%	Ni2	0.97 (0.63/0.33)	1.01 (0.71/0.29)	1.9	0.71	-0.16	-0.22
3/3@$a_{\rm STO}$	Ni IF	1.00 (0.77/0.23)	1.02 (0.80/0.21)	0.8	1.14	-0.12	-0.20
ϵ =1.7%	Ni IF-1	1.02 (0.81/0.21)	1.01 (0.80/0.21)	-0.3	1.20	-0.21	-0.20
LaNiO$_3$	Ni	1.00 (0.78/0.22)	1.00 (0.77/0.22)	0.0	1.12	-0.19	-0.20

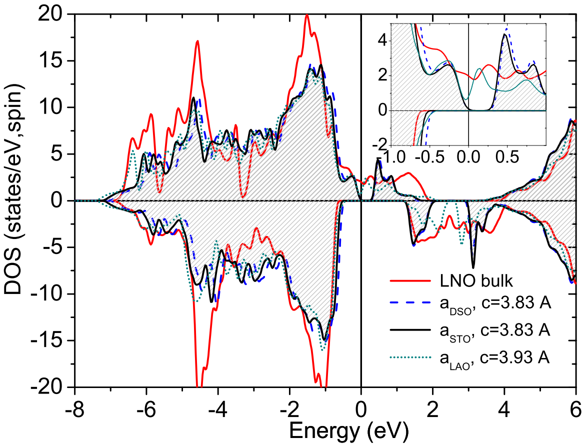

FIG. 3: (Color online) Total density of states for (LAO)$_1$/(LNO)$_1$ for the case of tensile (STO) (solid line, gray area), (DSO) (long-dashed blue line) and compressive strain (LAO) (short-dashed cyan line). Additionally, the DOS of monoclinic bulk LNO is shown with a red line. The inset shows a zoom-in around the Fermi level displaying the opening of a band gap for (LAO)$_1$/(LNO)$_1$ under tensile strain.

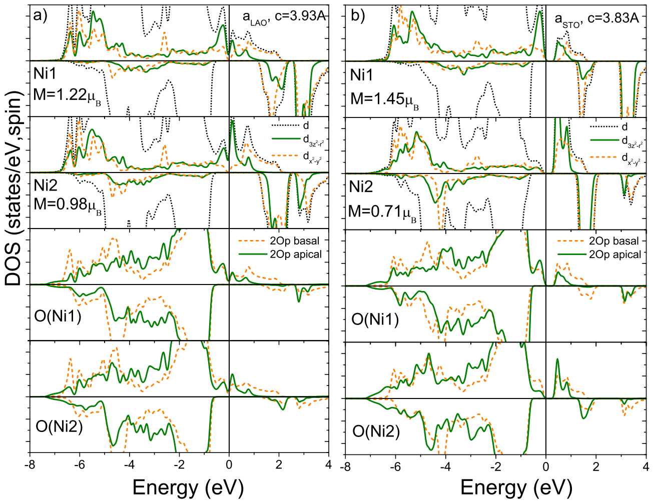

FIG. 4: (Color online) Projected density of states (PDOS) of Ni $3d$ states (black dotted line), $d_{3z^2-r^2}$ (green line) and $d_{x^2-y^2}$ orbitals (orange dashed line) in (LAO)$_1$/(LNO)$_1$ for (a) compressive (LAO) and (b) tensile (STO) strain. The lower panels show the PDOS of basal (orange dashed line) and apical (green line) oxygens. Note the charge disproportionation at the Ni sites and the reduced density at the apical oxygen sites.

In order to understand the origin of the distinct electronic behavior for tensile and compressive strain we analyze here the PDOS of the Ni $3d$ orbitals. Besides the filled t_{2g} orbitals there is a significant occupation of both e_g orbitals at the Ni sites (see Fig. 4) split into bonding (between -7 and -5 eV) and antibonding contributions (from -1 to 2 eV). The most striking effect for tensile strain is a charge disproportionation on the Ni sublattice, Ni^{3+} →Ni$^{3+\delta}$+Ni$^{3-\delta}$[31] where Ni1 has a stronger occupation of the e_g orbitals. The effect is most pronounced for the majority spin states with $0.87e$/$0.86e$ (Ni1) and $0.63e$/$0.71e$ (Ni2) in the $d_{3z^2-r^2}$/$d_{x^2-y^2}$ orbitals, respectively. The reduced occupation in the majority spin channel at Ni2 is partially compensated by a stronger filling of minority states at -4.3 eV. Altogether, the total difference in e_g occupation at the Ni1 (Ni$^{3-\delta}$) and Ni2 (Ni$^{3+\delta}$) sites is $\sim 0.2e$, but there is a significant difference in the magnetic moments $1.45\mu_{\rm B}$ (Ni1) and $0.71\mu_{\rm B}$ (Ni2) (for comparison, the magnetic moment in LNO bulk is $1.12\mu_{\rm B}$). Without the octahedral tilts and rotations such a state is reported at $U \geq 5$ eV.[7] A similar tendency for disproportionation was recently found in LNO films under tensile biaxial strain,[22,23] but here as a result of confinement in the LAO/LNO superlattice the effect is strongly enhanced leading to the opening of a gap of $\sim$0.5 eV at the Fermi level. Concerning the orbital polarization, the two sites show opposite, largely compensating tendencies: a slightly higher occupation of $d_{x^2-y^2}$ at Ni2 (+2.2%) and the reverse effect at Ni1 (-1.7%).

For compressive strain the charge disproportionation is noticeably reduced, reflected in a much smaller difference in the magnetic moments (1.22 μ_B at Ni1 and 0.98 μ_B at Ni2). We note that a non-disproportionated configuration lies only 12 meV/20-atom unit cell higher in energy. The broadening of the conduction band leads to an overlap with the valence band which closes the band gap with a dip in the PDOS at E_F. As a consequence of the distortion (elongation) of the NiO$_6$ octahedra discussed below, there is a stronger splitting between the $d_{3z^2-r^2}$ and $d_{x^2-y^2}$ states around E_F and an enhanced occupation of the $d_{3z^2-r^2}$ orbital in the majority spin channel [0.86e ($d_{3z^2-r^2}$) vs 0.76e ($d_{x^2-y^2}$) at Ni1 and 0.77e ($d_{3z^2-r^2}$) vs 0.72e ($d_{x^2-y^2}$) at Ni2]. Taking into account the occupation of the minority spin chanel the total number of electrons within the MT sphere is 1.06 ($d_{3z^2-r^2}$) vs. 0.98 ($d_{x^2-y^2}$) at Ni1 and 1.02 ($d_{3z^2-r^2}$) vs 0.98 ($d_{x^2-y^2}$) at Ni2, respectively. This results in an orbital polarization of -3.8% and -1.6%. We note that much higher values were obtained by Han emphet al.[8] by integrating only over the antibonding states from ~ -1.5 eV to E_F.

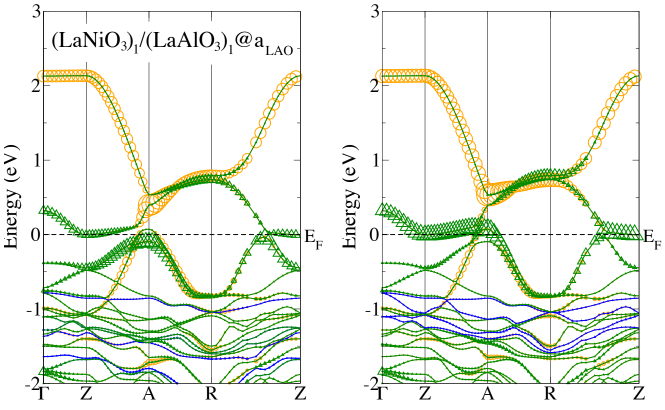

(a) Majority spin channel Ni 1

(b) Majority spin channel Ni 2

FIG. 5: (Color online) Majority spin band structure of (LAO)$_1$/(LNO)$_1$ under compressive strain (a_LAO). Note the reduced dispersion of the $d_{3z^2-r^2}$ band (green triangles) compared to bulk LNO caused by confinement and the opposite effect for the $d_{x^2-y^2}$ band (orange circles) due to the reduction of the in-plane lattice parameter.

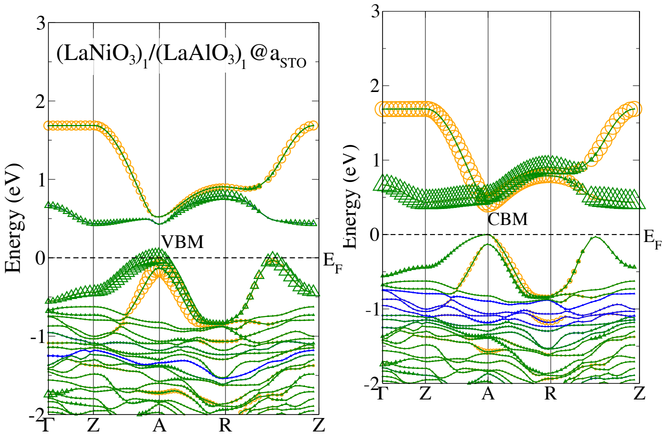

(a) Majority spin channel Ni 1

(b) Majority spin channel Ni 2

FIG. 6: (Color online) Majority spin band structure of (LAO)$_1$/(LNO)$_1$ under tensile (STO) strain. $d_{3z^2-r^2}$ and $d_{x^2-y^2}$ character is emphasized by green triangles and orange circles, respectively. The direct band gap opens at A with a valence band maximum (VBM) of predominantly Ni1 character and conduction band minimum (CBM) with mostly Ni2 contribution.

To gain more insight in the electronic structure of the (LaAlO$_3$)$_1$/(LaNiO$_3$)$_1$ superlattice, we have plotted in Fig. 5 and Fig. 6 the band structure in the majority spin channel for compressive (a_LAO) and tensile (a_STO) strain, respectively. As a consequence of confinement in the superlattice the $d_{3z^2-r^2}$band has a reduced dispersion compared to bulk LaNiO$_3$ (Fig. 2) and the degeneracy of the two e_g states at Γ is lifted with the $d_{3z^2-r^2}$state being 0.3 (a_LAO)/0.7 (a_STO) above E_F. The band structure around E_F is dominated by more localized $d_{3z^2-r^2}$ bands and strongly dispersive $d_{x^2-y^2}$ bands (especially for compressive strain) with dispersion of the latter mainly along $Z-A-R-Z$. As already mentioned in the discussion of the PDOS, there is a stronger splitting between $d_{3z^2-r^2}$ and $d_{x^2-y^2}$ states for a_LAO compared to a_STO. In contrast to bulk LNO (Fig. 2) a gap opens at A both for tensile and compresive strain. However, for compressive strain (a_LAO) the $d_{3z^2-r^2}$ band lies at the Fermi level along $Z-A$ and halfway along $R-Z$ causing a finite DOS at E_F. The upward shift of this band by $\sim$ 0.5 eV opens a band gap for a_STO. While the valence band maximum is mainly determined by $d_{3z^2-r^2}$ (and to a lesser extent $d_{x^2-y^2}$) states of Ni1 at A hybridized with p_z orbitals of the apical oxygen, the conduction band minimum is dominated by $d_{3z^2-r^2}$ states of Ni2, admixed with $d_{x^2-y^2}$and p_z bands of the respective apical oxygen. This results in a stronger suppression of ligand holes of the apical oxygen of Ni1.

The charge disproportionation at the Ni sites for a_STO is visible in the spatial distribution of holes shown in Fig. 7. In contrast to the three-dimensional network of holes on the basal and apical oxygens in bulk LNO [Fig. 1(b)], a striking feature in (LaAlO$_3$)$_1$/(LaNiO$_3$)$_1$ is the two- dimensional character of hole distribution within the LNO part of the superlattice due to a reduced number of holes in the p_z orbital of the apical oxygen for both tensile and compressive strain (see also PDOS of oxygen in Fig. 4). At the same time, the in-plane oxygen orbital occupancies are very similar to those in bulk LNO. As a measure of the number of holes in Table I we have determined the difference in filling between p_σ and the fully occupied p_π orbitals. We note that we consider here only the occupation within the MT sphere, which contains 60-70% of the total charge of oxygen. In bulk LNO there are 0.19 less electrons in the p_σ than in the p_π orbital within the MT. This number is reduced to $0.09-0.15e$ for the apical oxygens in the superlattice. The suppresion is strongest for the apical oxygen of Ni1 (Ni$^{3-\delta}$) which simultaneously has a higher $d_{3z^2-r^2}$ occupation. Thus the suppression of holes due to the stronger ionicity of the Al^{3+}-O-bond across the interface and the charge disporportionation at the Ni sites with more ionic and more covalent contributions at the two distinct Ni-sites are the crucial mechanisms in achieving an insulating state in

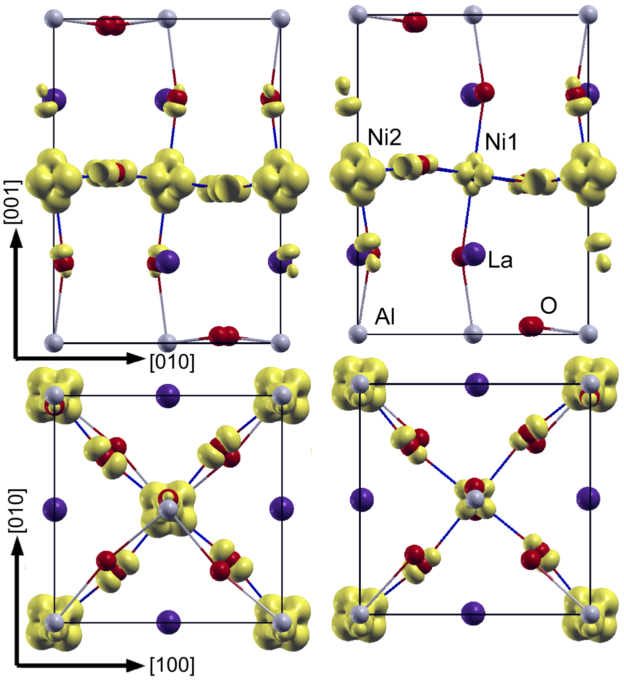

(a) a_{LAO} (b) a_{STO}

FIG. 7: (Color online) Electron density distribution of the unoccupied states integrated between $\mathrm{E_F}$ and $\mathrm{E_F}$+2.5 eV in $(\mathrm{LAO})_1/(\mathrm{LNO})_1$ for (a) compressive (LAO) and (b) tensile (STO) strain. Note the reduction in hole density on the apical oxygen between Ni and Al, as well as the charge disproportionation at the Ni sites for tensile strain. La, O, and Al ions are shown in purple, red, and light gray, respectively.

$(\mathrm{LaAlO_3})_1/(\mathrm{LaNiO_3})_1$.

B. $(\mathrm{LaAlO_3})_3/(\mathrm{LaNiO_3})_3$ superlattices

We turn now to the effect of LNO thickness on the electronic properties of the superlattice. The projected density of states (PDOS) at the Ni sites in $(\mathrm{LaAlO_3})_3/(\mathrm{LaNiO_3})_3$ at a_{STO} is displayed in Fig. 8. Unlike the $(\mathrm{LaAlO_3})_1/(\mathrm{LaNiO_3})_1$ system, there is a finite DOS at E_{F} at the Ni sites both in the IF and IF-1 layer and no evidence for charge disproportionation. The e_g states are nearly degenerate with a similar width as in the bulk and a small peak at E_{F}. Its character is predominantly $d_{3z^2-r^2}$ in the interface layer (IF) and Ni $d_{x^2-y^2}$ in IF-1 layer. As shown in the majority spin band structure in Fig. 9, these bands cross E_{F} at A [note that in $(\mathrm{LaAlO_3})_1/(\mathrm{LaNiO_3})_1$ a band gap opens at A]. The $d_{3z^2-r^2}$ bands of the two distinct layers (IF and IF-1) are split, with the IF band being narrower and lying lower in energy. In contrast to recent soft x-ray reflectivity measurements on $(\mathrm{LaAlO_3})_4/(\mathrm{LaNiO_3})_4$[24], we find only a small orbital polarization both in the interface (0.8%) and IF-1 (-0.3%) layers.

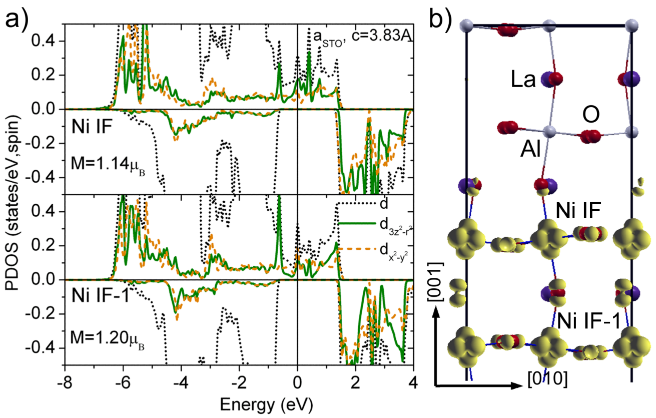

FIG. 8: (Color online) (a) Projected density of states (PDOS) of $3d$ states for Ni at interface (IF) and in the central layer (IF-1) in $(\mathrm{LaAlO_3})_3/(\mathrm{LaNiO_3})_3$ for tensile (STO) strain. Total $3d$, $d_{3z^2-r^2}$ and $d_{x^2-y^2}$ character are denoted by black dotted, green, and orange dashed line, respectivelyl. (b) Electron density distribution of unoccupied states (yellow) integrated between $\mathrm{E_F}$ and $\mathrm{E_F}$+2.5 eV. Note that only half of the simulation cell is shown. For color coding see Fig. 7.

Figure 8(b) shows the hole density distribution integrated between E_{F} and E_{F}+2.5 eV. Besides the similar hole density at the Ni sites independent of their position with respect to the interface, we observe again a reduced hole density at the apical oxygen at the interface. However, the O2p_z hole density is quickly restored to nearly bulk LNO behavior already in the next layer. This quick recovery of bulk LNO behavior at the apical oxygens away from the interface and the metallic state at the Ni sites with no evidence for charge disproportionation are instrumental for the insulator-to-metal transition in the $(\mathrm{LNO})_n/(\mathrm{LAO})_n$ SLs with increasing n, consistent with recent experiments.[9,10]

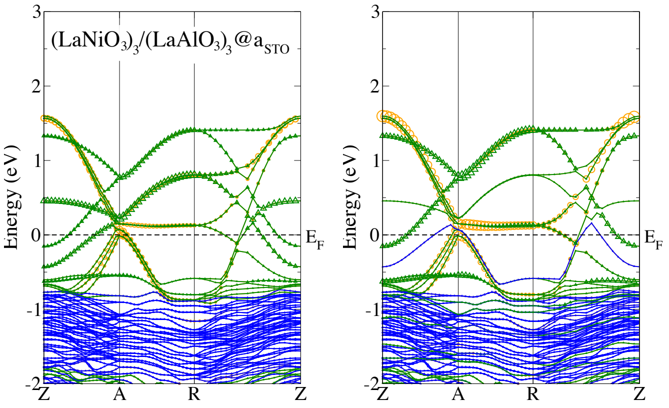

(a) Majority spin channel Ni IF (b) Majority spin channel Ni IF-1

FIG. 9: (Color online) Majority spin band structure of $(\mathrm{LaAlO_3})_3/(\mathrm{LaNiO_3})_3$ for tensile (STO) strain. Note the splitting of $d_{3z^2-r^2}$bands (green triangles) of Ni in the interface (IF) and (IF-1) layer, respectively. $d_{x^2-y^2}$ bands are emphasized by orange circles.

IV. STRAIN AND CONFINEMENT INDUCED LATTICE DEFORMATIONS

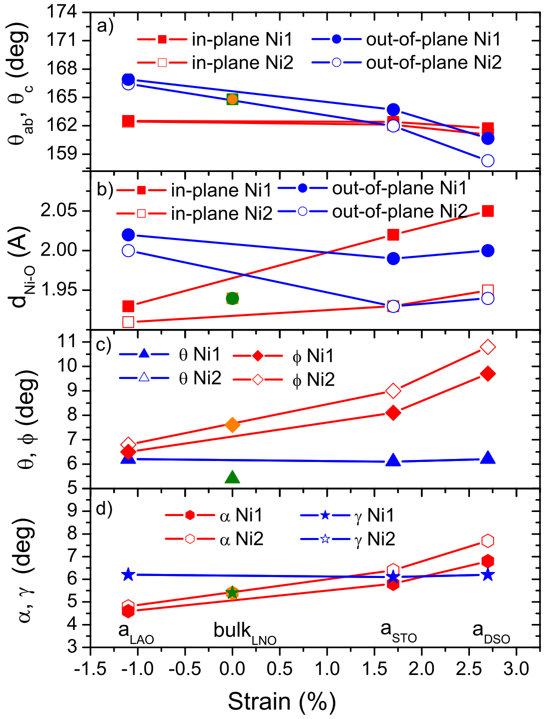

FIG. 10: (Color online) Strain dependence of the in-plane (red squares) and out-of-plane (blue circles) (a) bond angles and (b) Ni-O bond lengths in (LaAlO$_3$)$_1$/(LaNiO$_3$)$_1$; (c) NiO$_6$ octahedral rotation (θ) and tilt (ϕ) angles, and (d) Glazer's rotation angles α and γ. The symbols at 0% strain represent the bulk LNO values.

Not only the electronic but also the structural properties of the superlattice show a strongly asymmetric response to strain. The bond lengths and angles of the superlattices in comparison to bulk LNO and LAO are displayed in Table II and Fig. 10. For compressive strain the in-plane Ni-O bond length (1.92 Å) in (LaAlO$_3$)$_1$/(LaNiO$_3$)$_1$ is significantly shorter than the out-of-plane distance (2.01 Å), which is consistent with a volume-conserving tetragonal distortion and a crystal-field splitting between the $d_{3z^2-r^2}$ and $d_{x^2-y^2}$ orbitals observed in Fig. 4(a). In contrast, the charge disproportionation for tensile strain goes hand in hand with bond disproportionation driven by a *breathing* mode with two nearly regular octahedra with in-/out-of-plane cation-anion distances of 2.02/1.99 Å and 1.93/1.93 Å at the Ni1 and Ni2 sites at $a_{\rm STO}$, respectively.

As mentioned previously, in the bulk both LAO and LNO attain a rhombohedral structure with rotations of the octahedra around all three pseudocubic axes by $\alpha = \beta = \gamma = 3.04°$ (LAO) and 5.4° (LNO)[25]. This corresponds to Glazer's notation[26] (a^-, a^-, a^-). Recent DFT calculations[27] have found that under compressive strain the in-plane rotations of LAO are suppressed and the rotation pattern changes to (a^0, a^0, c^-). Vice versa for tensile strain the rotations are around the [110] direction (a^-, a^-, c^0). In contrast, an (a^-, a^-, c^-) pattern was reported in a combined XRD and DFT study[22] on strained LNO films with a strong reduction of $\gamma = 0.3 \pm 0.7°$ and enhanced $\alpha = 7.1 \pm 0.2°$ for tensile ($a_{\rm STO}$) and an opposite trend for compressive ($a_{\rm LAO}$) strain ($\alpha = 1.7 \pm 0.2°$ and $\gamma = 7.9 \pm 0.9°$). While the general pattern of octahedral rotations is preserved in the (LaAlO$_3$)$_1$/(LaNiO$_3$)$_1$ superlattice, the presence of the interface and the different strain state in the LAO and LNO part imposed by the substrate lead to significant changes of the absolute values of rotation angles compared to the individual phases described above. The rotational angle of the NiO$_6$ octahedra around [100] increases with strain from $\alpha \sim 4.7°$ ($a_{\rm LAO}$) to $\sim 6.1°$ ($a_{\rm STO}$) and $\sim 7.2°$ ($a_{\rm DSO}$), whereas γ remains constant $\sim 6.2°$. On the other hand, for the AlO$_6$ octahedra the rotational angle around [001] changes from $\gamma = 4.4°$ (compressive) to $\gamma \sim 2.5°$ (tensile strain).

The cation-oxygen-cation bond angles have a direct influence on the band width. In bulk LNO the Ni-O-Ni angle is 164.8°. In LAO, the deviation of the Al-O-Al angle from 180° is smaller (171.4°). For compressive strain: the out-of-plane Ni-O-Al angle in (LaAlO$_3$)$_1$/(LaNiO$_3$)$_1$ is increased to $\sim 166-167°$, while the in-plane Ni-O-Ni angle decreases to 163° (the in-plane Al-O-Al angle, 165.6°, is also reduced w.r.t. the bulk value). In contrast, for tensile strain both the in- (Ni-O-Ni) and out-of-plane (Ni-O-Al) bond angles are significantly reduced to $\sim$ 162° for $a_{\rm STO}$ and $\sim 161-162°$ for $a_{\rm DSO}$. The Al-O-Al is 167.3°, again smaller than the corresponding angle in bulk LAO (171.4°). The decrease of bond angles reduces the band width of $d_{3z^2-r^2}$ and $d_{x^2-y^2}$ bands between $E_{\rm F}$ and $E_{\rm F}$+4 eV, as can be seen in the PDOS in Fig. 4b). The Ni-O-Ni angle has been previously identified as the control parameter of the MIT in rare earth nickelates, where a smaller deviation from 180° favors Ni 3d-O2p hybridization and a metallic state, while a strong deviation leads to a MIT[3]. Indeed, the values we obtain for tensile strain ($160-162°$) are close to the Ni-O-Ni angles in PrNiO$_3$ (158.7°) and NdNiO$_3$ (157.1°)[25] that undergo a MIT.

In the (LaAlO$_3$)$_3$/(LaNiO$_3$)$_3$ superlattice under tensile strain ($a_{\rm STO}$) the octahedra are nearly regular with an in-/out-of-plane Ni-O bond length of 1.97/1.95 Å (IF) and 1.97/197 Å (IF-1), respectively. The pattern of octahedral rotations is preserved with almost identical absolute values of rotation angles compared to the (LaAlO$_3$)$_1$/(LaNiO$_3$)$_1$ at $a_{\rm STO}$. The out-of-plane Ni-O-Al (164°) and Ni-O-Ni (162°) and in-plane Ni-O-Ni angles $\sim$ 162° (IF)/163° (IF-1) are slightly higher than the ones for the (LaAlO$_3$)$_1$/(LaNiO$_3$)$_1$ superlattice in line with the metallicity of the system.

V. SUMMARY

While in the bulk LNO is metallic at all temperatures with degenerate e_g orbitals, we find that quantum confinement together with tensile strain allows to stabilize an insulating state in a (LaAlO$_3$)$_1$/(LaNiO$_3$)$_1$ superlattice. The charge disproportionation at the Ni sublattice with one strongly and one weakly magnetic Ni ion is fostered by the lattice response to strain, expressed in decreasing bond angles and enhanced tilt and rotation angles that reduce the band width. The charge

TABLE II: Ni-oxygen out-of-plane (d_{Ni-O^a}) and in-plane (d_{Ni-O^b}) distances, out-of-plane bond angle θ_c (Al-O-Ni), and in-plane angle θ_{ab} (Ni-O-Ni). Additionally, the rotation θ and tilt ϕ angles, as well as Glazer's rotation angles α and γ, are displayed.

		d_{Ni-O^a}	d_{Ni-O^b}	θ_c	θ_{ab}	θ	ϕ	α	γ
1/1@a_{LAO}	Ni1	2.02	1.93	166.9	162.5	6.2	6.5	4.6	6.2
ϵ =-1.1%	Ni2	2.00	1.91	166.4	162.5	6.2	6.8	4.8	6.2
1/1@a_{STO}	Ni1	1.99	2.02	163.7	162.4	6.1	8.1	5.8	6.1
ϵ =1.7%	Ni2	1.93	1.93	162.0	162.1	6.1	9.0	6.4	6.1
1/1@a_{DSO}	Ni1	2.00	2.05	160.7	161.7	6.2	9.7	6.8	6.2
ϵ =2.7%	Ni2	1.94	1.95	158.3	161.0	6.2	10.8	7.7	6.2
3/3@a_{STO}	Ni IF	1.95	1.97	163.9	162.3	6.2	8.1	5.7	6.2
ϵ =1.7%	Ni IF-1	1.97	1.97	162.4	162.6	6.4	8.8	6.2	6.4
$LaNiO_3$	Ni	1.94	1.94	164.8	164.8	5.4	7.6	5.4	5.4
$LaAlO_3$	Al	1.90	1.90	171.4	171.4	3.0	4.3	3.0	3.0

ordered state in the $(LaAlO_3)_1/(LaNiO_3)_1$ SL under tensile strain is characterized by two nearly regular octahedra with distinct bond lengths and hence a reduced crystal field splitting at the Ni-sites. On the other hand, under compressive strain bands broaden and close the band gap and CD is strongly inhibited. Expansion of the out-of-plane Ni-O bond length results in a crystal-field splitting between the $d_{x^2-y^2}$ and $d_{3z^2-r^2}$ orbitals and an energy lowering of the latter [see Fig. 4(b)]. This is similar to previous results for LNO films under compressive strain.[22]

LAO/LNO superlattices and strained LNO films show similar tilt patterns but different magnitude of octahedral rotations. This gives further evidence that the lattice response to strain in superlattices is very different from the one in thin films and thus provides a further possibility to tune the band width and the electronic behavior in transition metal oxides, as recently reported for LNO/SMO SLs.[28]

The large band width of the e_g states precludes significant changes in the orbital occupation via strain. The lack of lifting of orbital degeneracy is similar to other nickelates, e.g., $NdNiO_3$ where the MIT is not associated with orbital ordering.[29,30] Recently, Mazin emphet al.[4] proposed that the CO state in rare-earth nickelates gets gradually suppressed under pressure due to overlap of bands. In the confined $(LaAlO_3)_1/(LaNiO_3)_1$ we observe an analogous "melting" of the CD state as a function of strain: The significant difference in magnetic moments at the two distinct sites Ni1 and Ni2 sites at a_{STO} is gradually reduced for compressive strain.

The insulating state in the $(LaAlO_3)_1/(LaNiO_3)_1$ superlattice is achieved through a combination of charge disproportionation and a reduction of the hole density on the apical oxygens at the interface due to the ionic bonding to Al. The metallic behavior at the Ni sites and the hole density of the apical oxygen in inner layers is quickly restored in $(LaAlO_3)_3/(LaNiO_3)_3$ superlattices, in line with recent observations of a MIT with increasing LNO thickness.[9,10] We note that due to the presence of a surface, the mechanism of MIT in single layer films[12,13] may be different and requires further investigation.

R.P. acknowledges discussions with J. Freeland, J. Chakhalian, B. Keimer and R. J. Angel and thanks O. K. Andersen for several discussions on the band structures. We acknowledge financial support by the DFG (TRR80) and a grant for computational time at the Leibniz Rechenzentrum.

---

[*] Electronic address: rossitzap@lmu.de

[1] J. Chaloupka and G. Khaliullin, Phys. Rev. Lett. **100**, 016404 (2008).

[2] J. B. Torrance, P. Lacorre, A. I. Nazzal, E. J. Ansaldo, and C. Niedermayer, Phys. Rev. B **45**, 8209 (1992).

[3] M. Medarde, J. Phys.: Condens. Matter **9**, 1679 (1997).

[4] I. I. Mazin, D. I. Khomskii, R. Lengsdorf, J. A. Alonso, W. G. Marshall, R. M. Ibberson, A. Podlesnyak, M. J. Martínez-Lope, and M. M. Abd-Elmeguid, Phys. Rev. Lett. **98**, 176406 (2007).

[5] P. Hansmann, X. Yang, A. Toschi, G. Khaliullin, O. K. Andersen, and K. Held, Phys. Rev. Lett. **103**, 016401 (2009).

[6] P. Hansmann, A. Toschi, X. Yang, O. K. Andersen, and K. Held, Phys. Rev. B **82**, 235123 (2010).

[7] X. Yang and O. K. Andersen, Thickness and Cation Control of Conduction in Nickelate Heterostructures, Annual Report of the Max-Planck Institute for Solid State Research 2010, 74-79, http://www.fkf.mpg.de/andersen/ and http://online.kitp.ucsb.edu/online/materials10/andersen/ (2011).

[8] M. J. Han, C. A. Marianetti, and A. J. Millis, Phys. Rev. B **82**, 134408 (2010).

[9] J. Liu, S. Okamoto, M. van Veenendaal, M. Kareev, B. Gray, P. Ryan, J. W. Freeland, and J. Chakhalian, Phys. Rev. B **83**, 161102 (2011).

[10] A. V. Boris, Y. Matiks, E. Benckiser, A. Frano, P. Popovich, V. Hinkov, P. Wochner, M. Castro-Colin, E. Detemple, V. K. Malik, C. Bernhard, T. Prokscha, A. Suter, Z. Salman, E. Morenzoni, G. Cristiani, H. -U. Habermeier, and B. Keimer, Science **332**, 937 (2011).

[11] S. J. May, T. S. Santos, and A. Bhattacharya, Phys. Rev. B **79**, 115127 (2009).

[12] R. Scherwitzl, S. Gariglio, M. Gabay, P. Zubko, M. Gibert, and J.-M. Triscone, Phys. Rev. Lett. **106**, 246403 (2011).

[13] J. Son, P. Moetakef, J. M. LeBeau, D. Ouellette, L. B. amd S. J. Allen, and S. Stemmer, Appl. Phys. Lett **96**, 062114 (2010).

[14] V. Pardo and W. E. Pickett, Phys. Rev. Lett. **105**, 266402 (2010).

[15] V. V. Poltavets, K. A. Lokshin, A. H. Nevidomskyy, M. Croft, T. A. Tyson, J. Hadermann, G. Van Tendeloo, T. Egami, G. Kotliar, N. ApRoberts-Warren, A. P. Dioguardi, N. J. Curro, and M. Greenblatt, Phys. Rev. Lett. **104**, 206403 (2010).

[16] P. Blaha, K. Schwarz, G. K. H. Madsen, D. Kvasnicka, and J. Luitz, *Wien2k, an augmented plane wave plus local orbitals program for calculating crystal properties*, (Karlheinz Schwarz, Technische Universität Wien, Austria, 2001).

[17] J. P. Perdew, K. Burke, and M. Ernzerhof, Phys. Rev. Lett. **77**, 3865 (1996).

[18] V. I. Anisimov, I. V. Solovyev, M. A. Korotin, M. T. Czyżyk, and G. A. Sawatzky, Phys. Rev. B **48**, 16929 (1993).

[19] J. W. Freeland, J. Liu, M. Kareev, B. Gray, J. Kim, P. Ryan, R. Pentcheva, and J. Chakhalian, Europhys. Lett., in press. (2011).

[20] T. Mizokawa, A. Fujimori, T. Arima, Y. Tokura, N. Mōri, and J. Akimitsu, Phys. Rev. B **52**, 13865 (1995).

[21] V. I. Anisimov, D. Bukhvalov, and T. M. Rice, Phys. Rev. B **59**, 7901 (1999).

[22] S. J. May, J.-W. Kim, J. M. Rondinelli, E. Karapetrova, N. A. Spaldin, A. Bhattacharya, and P. J. Ryan, Phys. Rev. B **82**, 014110 (2010).

[23] J. Chakhalian, J. M. Rondinelli, J. Liu, B. A. Gray, M. Kareev, E. J. Moon, N. Prasai, J. L. Cohn, M. Varela, I. C. Tung, M. J. Bedzyk, S. G. Altendorf, F. Strigari, B. Dabrowski, L. H. Tjeng, P. J. Ryan, J. W. Freeland, Phys. Rev. Lett. **107**, 116805 (2011).

[24] E. Benckiser, M. Haverkort, S. Brück, E. Goering, S. Macke, A. Frano, X. Yang, O. Andersen, G. Cristiani, H.-U. Habermeier, A. V. Boris, I. Zegkinoglou, P. Wochner, H. -J. Kim, V. Hinkov, and B. Keimer, Nat. Mat **10**, 189 (2011).

[25] J. L. García-Muñoz, J. Rodríguez-Carvajal, P. Lacorre, and J. B. Torrance, Phys. Rev. B **46**, 4414 (1992).

[26] A. M. Glazer, Acta. Cryst. Section B **28**, 3384 (1972).

[27] A. J. Hatt and N. A. Spaldin, Phys. Rev. B **82**, 195402 (2010).

[28] S. J. May, C. R. Smith, J.-W. Kim, E. Karapetrova, A. Bhattacharya, and P. J. Ryan, Phys. Rev. B **83**, 153411 (2011).

[29] V. Scagnoli, U. Staub, A. M. Mulders, M. Janousch, G. I. Meijer, G. Hammerl, J. M. Tonnerre, and N. Stojic, Phys. Rev. B **73**, 100409 (2006).

[30] J. L. García-Muñoz, M. A. G. Aranda, J. A. Alonso, and M. J. Martínez-Lope, Phys. Rev. B **79**, 134432 (2009).

[31] Although due to covalency the Ni $3d$ band occupation is a mixture of $3d^7$ and $3d^8$L ground state, we use here for clarity the formal oxidation state of Ni.